Synthesis, Photoluminescence, and Electrochromism of Polyamides Containing (3,6-Di-*tert*-butylcarbazol-9-yl)triphenylamine Units

HUI-MIN WANG,[1] SHENG-HUEI HSIAO,[1] GUEY-SHENG LIOU,[2] CHIEH-HSIANG SUN[3]

[1]Department of Chemical Engineering and Biotechnology, National Taipei University of Technology, Taipei 10608, Taiwan

[2]Institute of Polymer Science and Engineering, National Taiwan University, Taipei 10617, Taiwan

[3]Department of Chemical Engineering, Tatung University, Taipei 10451, Taiwan

Received 19 June 2010; accepted 1 August 2010
DOI: 10.1002/pola.24269
Published online 7 September 2010 in Wiley Online Library (wileyonlinelibrary.com).

ABSTRACT: A new carbazole-derived, triphenylamine (TPA)-containing aromatic dicarboxylic acid monomer, 4,4′-dicarboxy-4″-(3,6-di-*tert*-butylcarbazol-9-yl)TPA, was synthesized, and it led to a series of electroactive aromatic polyamides with main-chain TPA and pendent 3,6-bis(*tert*-butyl)carbazole units by reacting it with various aromatic diamines via the phosphorylation polyamidation technique. The polyamides were amorphous with good solubility in many organic solvents and could be solution-cast into flexible and strong films. They showed high glass-transition temperatures (282–335 °C) and high thermal stability (10% weight loss temperatures >480 °C). The electroactive polymer films had well-defined and reversible redox couples with good cycle stability in acetonitrile solutions. The polymer films also exhibited fluorescent and multielectrochromic behaviors. The anodically electrochromic polyamide films had moderate coloration efficiency (~100 cm^2/C) and high optical contrast ratio of transmittance change ($\Delta\%T$) up to 47% at 813 nm and 48% at 414 nm for the green coloring. After hundreds of cyclic switches, the polymer films still retained good redox and electrochromic activity. © 2010 Wiley Periodicals, Inc. J Polym Sci Part A: Polym Chem 48: 4775–4789, 2010

KEYWORDS: carbazole; electrochemistry; electrochromism; fluorescence; polyamides; redox polymers; spectroelectrochemistry; triphenylamine

INTRODUCTION Electrochromism is defined as a reversible and visible change in the transmittance and/or reflectance of a material as the result of electrochemical oxidation or reduction.[1] This is an intriguing phenomenon for which there might be a wide range of applications, including optical switching devices, color displays, smart windows, sensors, memory elements, and camouflage materials.[2] The property of electrochromism is not unique to conducting polymers, but is found in a variety of organic and inorganic materials.[3] Significant effort has been put forth on electrochromic devices based on inorganic electrochromic systems such as tungsten oxide (WO_3) and nickel oxide (NiO or Ni_2O_3).[4] π-Conjugated organic polymers present improved processability and better color tunability than their inorganic and molecular counterparts.[5] Electrochemical switching in conjugated polymers, providing electrochromism, is a phenomenon possible to achieve in robust device architectures operated at low voltages. Considerable effort in the Reynolds group has been focused on the understanding and the tailoring of electrochromic properties in conjugated polymers such as poly(3,4-alkylenedioxythiophene)s[6] and poly(3,4-alkylenedioxypyrrole)s.[7] Many conjugated polymer systems exhibiting attractive electrochromic performance have also been explored by other research teams.[8] The electroactive and conjugated polymers generally demonstrated superior electrochromic properties, such as a fast switching capability, high contrast ratio, high coloration efficiency (CE), and good long-term stability. Despite the attractive electrochromic performance of many conjugated polymers, most of them were prepared by electrochemical polymerization and in some cases were insoluble after deposition on the electrode surface, which may hamper their applications for large area devices. In addition, long-term stability of conjugated polymers remains a problem. For example, poly(3,4-ethylenedioxythiophene) degrades over time if exposed to light or heat. Therefore, there remains a great need to develop polymeric electrochromics with useful electrochromic properties as well as good processability and high thermal stability.

Wholly aromatic polyamides (aramids) are considered to be high-performance polymers because of their outstanding thermal and mechanical properties.[9] A major problem with aramids having high softening temperatures (particularly those prepared with *p*-phenylene units) is their low solubility and resultant difficulty in fabrication. One approach to solving this has been the incorporation of bulky groups in the main chain or as the pendent groups.[10] There is continuously a huge effort directed toward expanding the application of the aromatic

Additional Supporting Information may be found in the online version of this article. Correspondence to: S.-H. Hsiao (E-mail: shhsiao@ntut.edu.tw)
Journal of Polymer Science: Part A: Polymer Chemistry, Vol. 48, 4775–4789 (2010) © 2010 Wiley Periodicals, Inc.

polyamides as optically active materials, luminescent and electroactive films, gas or ion-exchange membranes, etc., by incorporating new chemical functionalities in the polyamide backbone or lateral structure.[11]

Triarylamine derivatives are well-known for their electroactive and photoactive properties that may find optoelectronic applications as photoconductors, hole-transporters, and light-emitters.[12] Polymers bearing triarylamine units are receiving considerable interest as ideal hole-transporting materials in various optoelectronic device applications such as organic light-emitting diodes (OLEDs) because of the strong electron-donating and hole-transporting/injecting properties of triarylamine units.[13] Triarylamines can be easily oxidized to form stable radical cations, and the oxidation process is always associated with a strong change of coloration.[14] In recent years, we have initiated a program aimed at the design and synthesis of high-performance polymers (typically, aromatic polyamides and polyimides) carrying the triarylamine unit as an electrochromic functional moiety.[15] The obtained polymers possessed characteristically high molecular weights and high thermal stability. Because of the incorporation of packing-disruptive, propeller-shaped triarylamine units along the polymer backbone, most of these polymers exhibited good solubility in polar organic solvents and could be easily solvent cast into morphologically stable films.

Carbazole is also a well-known hole-transporting and light-emitting unit. Carbazole could be easily functionalized at its 3,6-, 2,7-, or *N*-positions and then covalently linked to polymeric systems, both in the main chain as building blocks and in a side chain as pending groups.[16] Polymers containing carbazole moieties in the main chain or side chain have attracted much attention because of their unique properties, which allow various optoelectronic applications such as photoconductive, electroluminescent, electrochromic, and photorefractive materials.[17] In a previous publication,[15c] we have reported on the polyamides bearing main-chain triphenylamine (TPA) and pendent carbazole units from the dicarboxylic acid monomer 4,4′-dicarboxy-4″-*N*-carbazolyltriphenylamine. The polyamides could afford amorphous and high-T_g films with useful mechanical properties (e.g., flexibility). They also reveal good redox stability for the first oxidation state, and the oxidation process is accompanied with a noticeable change of the coloration. However, the second oxidation process of these polymers is not reversible, possibly because of the electrochemical coupling of carbazoles through the active C-3 and C-6 sites. It has been demonstrated that introduction of bulky groups on the electrochemically active sites (C-3 and C-6) of carbazole leads to enhanced electrochemical and morphological stability.[18] In this article, a molecular-design strategy to retain the useful properties of such polymers while enhancing the redox stability by substitution of the C-3 and C-6 positions of the carbazole unit with bulky *tert*-butyl groups is reported. Thus, a novel carbazole-derived, TPA-containing dicarboxylic acid monomer **5** was synthesized, and it led to a series of novel aromatic polyamides with main-chain TPA and pendent 3,6-bis(*tert*-butyl)carbazole units. The *tert*-butyl groups are expected to increase the solubility and to give extra electrochemical stability of the resulting polymers.

EXPERIMENTAL

Materials

As reported previously,[15c] 4,4′-dicarboxy-4″-*N*-carbazolyltriphenylamine was synthesized by alkaline hydrolysis of 4,4′-dicyano-4″-*N*-carbazolyltriphenylamine resulting from the nucleophilic aromatic substitution reaction of *p*-fluorobenzonitrile with the amide ion of *N*-(4-aminophenyl)carbazole formed *in situ* by the treatment with sodium hydride (NaH). According to a previously published procedure,[19] 2-trifluoromethyl-4,4′-diaminodiphenyl ether (**6c**; mp: 112–113 °C) was synthesized by the nucleophilic chloro-displacement reaction of 2-chloro-5-nitrobenzotrifluoride with 4-nitrophenol in the presence of potassium carbonate, followed by the hydrazine Pd/C-catalyzed reduction of the intermediate dinitro compound. 4,4′-Diamino-4″-*tert*-butyltriphenylamine (**6e**; mp: 113–115 °C) was synthesized by the cesium fluoride-mediated condensation of 4-*tert*-butylaniline with *p*-fluoronitrobenzene, followed by a palladium-catalyzed hydrazine reduction.[15b] The other aromatic diamines such as *p*-phenylenediamine (**6a**), 4,4′-diaminodiphenyl ether (**6b**), and 9,9-bis(4-aminophenyl)fluorene (**6d**) were supplied from TCI (Tokyo Chemical Industry) and used without further purification. NMP was dried over calcium hydride for 24 h, distilled under reduced pressure, and stored over 4 Å molecular sieves in a sealed bottle. Commercially obtained calcium chloride ($CaCl_2$) was dried under vacuum at 180 °C for 8 h prior to use. Tetrabutylammonium perchlorate, Bu_4NClO_4, was recrystallized from ethyl acetate under nitrogen atmosphere and then dried *in vacuo* prior to use. All other reagents and solvents were used as received from commercial sources.

Monomer Synthesis

9-(4-Nitrophenyl)carbazole (1)

According to the synthesis procedure reported previously,[15c] Compound **1** (mp: 208–209 °C) was prepared by nucleophilic fluoro-displacement reaction of *p*-fluoronitrobenzene with carbazole in the presence of cesium fluoride (CsF).

IR (KBr): 1594, 1326 cm^{-1} (NO_2 stretch). ^1H NMR (DMSO-d_6, δ, ppm): 7.36 (t, 2H, H_e), 7.48 (t, 2H, H_d), 7.56 (d, 2H, H_c), 7.98 (d, 2H, H_b), 8.28 (d, 2H, H_f), 8.50 (d, 2H, H_a). ^{13}C NMR (DMSO-d_6, δ, ppm): 109.8 (C^6), 120.6 (C^8), 121.0 (C^9), 123.4 (C^{10}), 125.6 (C^2), 126.6 (C^7), 126.9 (C^3), 139.2 (C^5), 142.9 (C^1), 145.4 (C^4). The IR, ^1H NMR, and ^{13}C NMR spectra of compound **1** are illustrated in the Supporting Information (see Supporting Information Figs. S1 and S2).

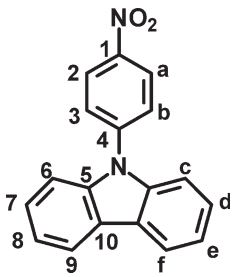

3,6-Di-tert-butyl-9-(4-nitrophenyl)carbazole (2)

To a solution of Compound **1** (14.4 g; 0.05 mol) in 140 mL of *tert*-butyl chloride, anhydrous $AlCl_3$ (0.8 g;

0.006 mol) was added slowly with stirring in four portions over a 30-min period. After the addition, the solution became dense and a large amount of hydrochloric acid was liberated. The solution was stirred vigorously at room temperature for 24 h. Then, cold water was added to decompose trace $AlCl_3$. The solid precipitated from the solution was collected by filtration and washed thoroughly with water. Recrystallization from DMF yielded 16 g (86% in yield) of nitro compound **2** as yellow needles with mp = 236–237 °C (ref. 20: 234–235 °C) measured by DSC at 10 °C/min.

IR (KBr): 2952 cm^{-1} (*t*-butyl C–H stretch), 1592, 1336 cm^{-1} (NO_2 stretch). ^1H NMR (500 MHz, DMSO-d_6, δ, ppm): 1.40 (s, 18H, H_f), 7.49 (d, J = 8.7 Hz, 2H, H_d), 7.52 (d, J = 8.7 Hz, 2H, H_c), 7.96 (d, J = 8.9 Hz, 2H, H_b), 8.33 (s, 2H, H_e), 8.48 (d, J = 9.0 Hz, 2H, H_a). ^{13}C NMR (125 MHz, DMSO-d_6, δ, ppm): 31.64 (C^{12}), 34.47 (C^{11}), 109.30 (C^6), 116.88 (C^9), 123.60 (C^8), 123.97 (C^7), 125.49 (C^3), 126.21 (C^2), 137.50 (C^5), 143.68 (C^{10}), 144.86 (C^1), 150.91 (C^4). The IR, ^1H NMR, and ^{13}C NMR spectra of Compound **2** are shown in the Supporting Information (see Supporting Information Figs. S1 and S3).

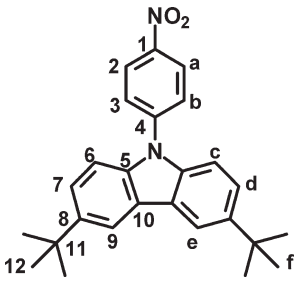

3,6-Di-tert-butyl-9-(4-aminophenyl)carbazole (3)

In a 1 L round-bottom flask equipped with a stirring bar, 8.0 g (0.02 mol) of Compound **2** and 0.2 g of 10% Pd/C were dissolved/suspended in 800 mL of ethanol. The suspension solution was heated to reflux, and 6 mL of hydrazine monohydrate was added slowly to the mixture, then the solution was stirred at reflux temperature. After a further 9 h of reflux, the solution was filtered hot to remove Pd/C, and the filtrate was then cooled to precipitate a gray-colored product. The product was collected by filtration and dried *in vacuo* at 80 °C to give 6.0 g (81% in yield) of gray-colored crystals with a mp of 223–224 °C measured by DSC at 2 °C/min.

IR (KBr): 3442, 3336 cm^{-1} (*N*–H stretch). ^1H NMR (500 MHz, DMSO-d_6, δ, ppm): 1.41 (s, 18H, H_f), 5.37 (s, 2H, $-NH_2$), 6.78 (d, 2H, H_a), 7.15-7.17 (m, 4H, H_b + H_c), 7.43 (d, 2H, H_d), 8.22 (s, 2H, H_e). ^{13}C NMR (125 MHz, DMSO-d_6, δ, ppm): 31.8 (C^{12}), 34.3 (C^{11}), 108.9 (C^6), 114.6 (C^9), 116.3 (C^{10}), 122.1 (C^2), 123.3 (C^7), 125.0 (C^8), 127.4 (C^3), 139.3 (C^5), 141.6 (C^4), 148.1 (C^1). The IR, ^1H NMR, and ^{13}C NMR spectra of Compound **3** are included in the Supporting Information (see Supporting Information Figs. S1 and S4).

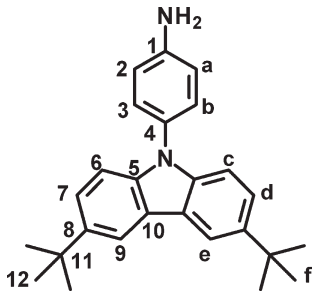

4,4′-Dicyano-4″-(3,6-di-tert-butylcarbazol-9-yl)TPA (4)

In a 250-mL three-neck round-bottom flask equipped with a stirring bar, a mixture of 14.8 g (0.042 mol) of Compound **3**, 10.2 g (0.084 mol) of *p*-fluorobenzonitrile, 12.8 g (0.084 mol) of CsF, and 4.4 g (0.017 mol) of 18-crown-6 in 80 mL of dry DMSO was heated with stirring at 150 °C for 24 h under nitrogen atmosphere. After cooling, the reaction mixture was poured into 300 mL of stirred methanol slowly, and the crude product was collected by filtration and then recrystallized from DMF/methanol to give yellowish needles (11.6 g, 48% yield) with an mp of 341–343 °C (by DSC at a scan rate of 2 °C/min).

IR (KBr): 2952 cm^{-1} (*t*-butyl C–H stretch), 2217 cm^{-1} (C≡N). ^1H NMR (500 MHz, DMSO-d_6, δ, ppm): 1.50 (s, 18H, H_h), 7.24 (d, J = 8.7 Hz, 4H, H_b), 7.35 (d, J = 8.6 Hz, 2H, H_c), 7.43 (d, J = 8.6 Hz, 2H, H_e), 7.54 (d, J = 8.7 Hz, 2H, H_f), 7.61 (d, J = 8.9 Hz, 2H, H_d), 7.62 (d, J = 8.6 Hz, 4H, H_a), 8.17 (s, 2H, H_g). ^{13}C NMR (125 MHz, DMSO-d_6, δ, ppm): 31.96 (C^{14}), 34.73 (C^{13}), 106.33 (C^1), 109.03 (C^{10}), 116.38 (C^{15}), 118.75 (–CN), 123.18 (C^3), 123.57 (C^{11}), 123.69 (C^{16}), 127.73 (C^6), 128.07 (C^7), 133.71(C^2), 136.20 (C^8), 138.87 (C^{12}), 143.27 (C^5), 143.33 (C^9), 150.06 (C^4). The IR, ^1H NMR, and ^{13}C NMR spectra of Compound **4** can be seen in the Supporting Information (Supporting Information Figs. S1 and S5).

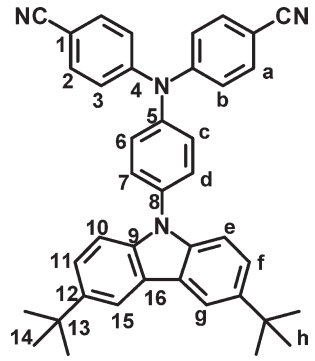

4,4′-Dicarboxy-4″-(3,6-di-tert-butylcarbazol-9-yl)TPA (5)

A mixture of 12 g of potassium hydroxide and 4.5 g of the dinitrile compound **4** in 150 mL ethanol and 50 mL of distilled water was stirred at about 100 °C until no further ammonia was generated. The time taken to reach this stage was about a week. The solution was cooled, and the pH value was adjusted by hydrochloric acid to near 3. The yellowish precipitate was filtered, washed thoroughly with water, and recrystallized from acetic acid to afford 4.0 g (86% in yield) of yellow crystals with mp of 364–366 °C (by DSC at a scan rate of 2 °C/min).

IR (KBr): 2400–3400 cm^{-1} (O–H), 2952 cm^{-1} (*t*-butyl C–H stretch), 1687 (C=O stretch). ^1H NMR [500 MHz, DMSO-d_6, δ, ppm; for the peak assignments, see Fig. 1(a)]: 1.40 (s, 18H, H_h), 7.19 (d, J = 7.6 Hz, 4H, H_b), 7.35 (d, J = 8.4 Hz, 2H, H_c), 7.38 (d, J = 8.5 Hz, 2H, H_e), 7.48 (d, J = 8.7 Hz, 2H, H_f), 7.62 (d, J = 8.7 Hz, 2H, H_d), 7.93 (d, J = 8.8 Hz, 4H, H_a), 8.28 (s, 2H, H_g). ^{13}C NMR [125 MHz, DMSO-d_6, δ, ppm; for the peak assignments, see Fig. 1(b)]: 31.72 (C^{14}), 34.39 (C^{13}), 109.10 (C^{10}), 116.55 (C^{15}), 122.79 (C^3), 122.99 (C^{16}), 123.57 (C^{11}), 125.00 (C^1), 127.11 (C^6), 127.58 (C^7), 131.04 (C^2), 134.00 (C^8), 138.36 (C^{12}), 142.50 (C^9), 144.09 (C^5), 150.17 (C^4), 166.70 (–COOH).

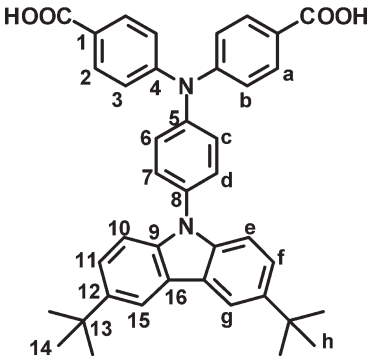

Polymer Synthesis

The synthesis of polyamide **7a** was used as an example to illustrate the general synthetic route. A mixture of 0.489 g (0.8 mmol) of dicarboxylic acid monomer **5**, 0.086 g (0.8 mmol) of *p*-phenylenediamine (**6a**), 0.15 g of anhydrous calcium chloride, 0.8 mL of triphenyl phosphite (TPP), 0.2 mL of pyridine, and 1.0 mL of NMP was heated with stirring at 120 °C for 3 h. The resulting viscous solution was poured slowly with stirring into 150 mL of methanol, giving rise to a tough, fibrous precipitate. The precipitated product was collected by filtration, washed repeatedly with methanol and hot water, and dried to give a quantitative yield of polyamide **7a**. The inherent viscosity of the polymer was 0.61 dL/g, measured in dimethylacetamide (DMAc; containing 5 wt % LiCl) at a concentration of 0.5 g/dL at 30 °C. The IR spectrum of **7a** (film) exhibited characteristic amide absorption bands at 3300 cm^{-1} (amide *N*–H stretch) and 1653 cm^{-1} (amide carbonyl stretch).

^1H NMR (500 MHz, DMSO-d_6, δ, ppm; for the peak assignments, see Fig. 2): 1.43 (s, 18H, H_h), 7.28 (d, 4H, H_b), 7.39 (d, 4H, H_c + H_e), 7.50 (d, 2H, H_f), 7.65 (d, 2H, H_d), 7.75 (s, 4H, H_i), 8.00 (d, 4H, H_a), 8.29 (s, 2H, H_g), 10.19 (s, 1H, amide).

Preparation of the Polyamide Films

A solution of the polymer was made by dissolving about 0.6 g of the polyamide sample in 10 mL of DMAc. The homogeneous solution was poured into a 7-cm glass Petri dish, which was placed in a 90 °C oven overnight to remove most of the solvent. The cast film was then released from the glass substrate and was further dried *in vacuo* at 160 °C for 8 h.

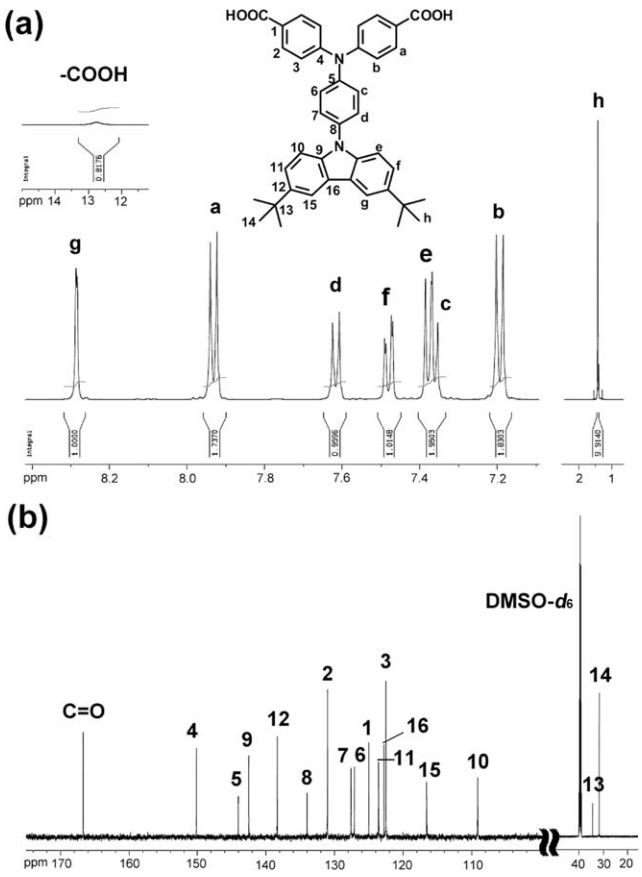

FIGURE 1 (a) ^1H NMR and (b) ^{13}C NMR spectra of the dicarboxylic acid monomer **5** in DMSO-d_6.

The obtained films were about 50–60 μm thick and were used for X-ray diffraction measurements, solubility tests, and thermal analyses.

Measurements

IR spectra were recorded on a Horiba FT-720 FTIR spectrometer. Elemental analyses were run in a Heraeus VarioEL III CHNS elemental analyzer. ^1H and ^{13}C NMR spectra were measured on a Bruker Avance 500 FT-NMR system with TMS as an internal standard. The inherent viscosities were determined with a Cannon-Fenske viscometer at 30 °C. Weight-average molecular weights (M_w) and number-average molecular weights (M_n) were obtained via GPC on the basis of polystyrene calibration using Waters 2410 as an apparatus and THF as the eluent. Wide-angle X-ray diffraction (WAXD) measurements were performed at room temperature (~25 °C) on a Shimadzu XRD-6000 X-ray diffractometer with a graphite monochromator (operating at 40 kV and 30 mA), using nickel-filtered Cu Kα radiation (λ = 1.5418 Å). The scanning rate was 2°/min over a range of 2θ = 10–40°. TGA was performed with a Perkin–Elmer Pyris 1 TGA. Experiments were carried out on ~4–6 mg of samples heated in flowing nitrogen or air (flow rate = 40 cm^3/min) at a heating rate of 20 °C/min. DSC analyses were performed on a Perkin–Elmer Pyris 1 DSC at a scan rate of 20 °C/min in flowing nitrogen. TMA was determined with a Perkin–

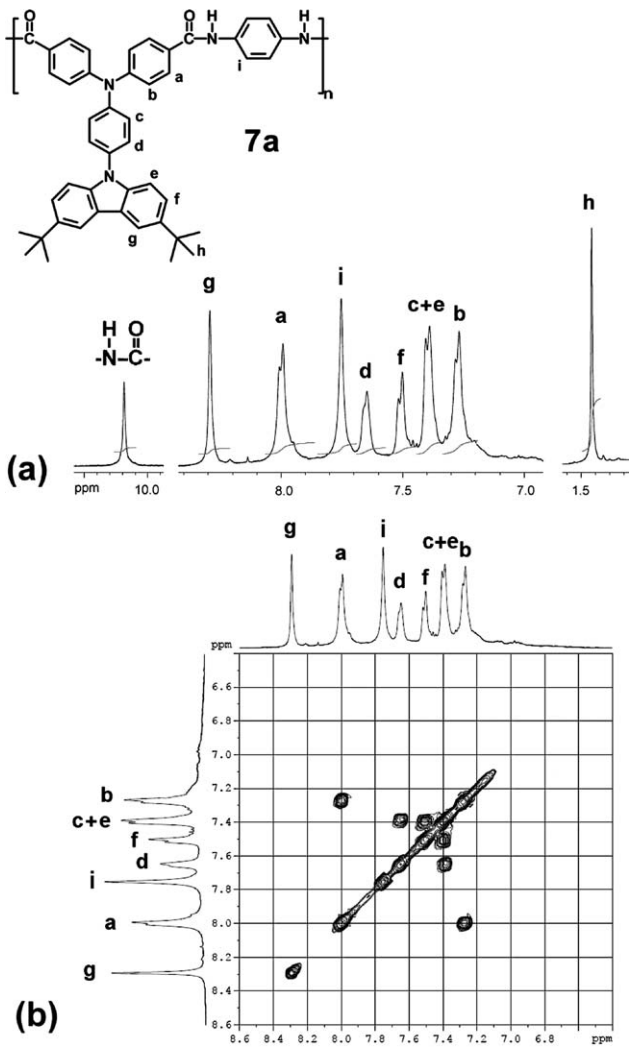

FIGURE 2 (a) ^{1}H NMR spectrum and (b) aromatic portion of the ^{1}H–^{1}H COSY spectrum of polyamide **7a** in DMSO-d_6.

Elmer TMA 7 instrument. The TMA experiments were carried out from 50 to 400 °C at a scan rate of 10 °C/min with a penetration probe 1.0 mm in diameter under an applied constant load of 10 mN. Softening temperatures (T_s) were taken as the onset temperatures of probe displacement on the TMA traces. UV–vis spectra of the polymer films were recorded on an Agilent 8453 UV–Visible spectrometer. PL spectra were measured with a Varian Cary Eclipse fluorescence spectrophotometer. Fluorescence quantum yields (Φ_F) values of the samples in NMP were measured by using quinine sulfate in 1 N H_2SO_4 as a reference standard (Φ_F = 54.6%).[21] Electrochemistry was performed with a CHI 750A electrochemical analyzer. CV was conducted with the use of a three-electrode cell in which indium tin oxide (ITO; polymer films area about 0.8 cm × 1.25 cm) was used as a working electrode. A platinum wire was used as an auxiliary electrode. All cell potentials were taken with the use of a homemade Ag/AgCl, KCl (sat.) reference electrode. Ferrocene was used as an external reference for calibration (+0.48 V vs. Ag/AgCl). Voltammograms are presented with the positive potential pointing to the left and with increasing anodic currents pointing downwards. Spectroelectrochemistry analyses were carried out with an electrolytic cell, which was composed of a 1-cm cuvette, ITO as a working electrode, a platinum wire as an auxiliary electrode, and a Ag/AgCl reference electrode. Absorption spectra in the spectroelectrochemical experiments were measured with an Agilent 8453 UV–Visible diode array spectrophotometer. Color measurements were performed by using Konica Minolta CS-200 ChromaMeter with viewing geometry as recommended by Commision Internationale de I'Eclairage.

RESULTS AND DISCUSSION

Monomer Synthesis

The new dicarboxylic acid monomer, 4,4′-dicarboxy-4″-(3,6-di-*tert*-butylcarbazol-9-yl)TPA (**5**), was synthesized by a five-step reaction sequence as shown in Scheme 1. In the first step, the intermediate compound, *N*-(4-nitrophenyl)carbazole (**1**) was synthesized by nucleophilic aromatic fluoro-displacement reaction of *p*-fluoronitrobenzene with carbazole in the presence of CsF.[15c] Friedel–Crafts alkylation of Compound **1** with *tert*-butyl chloride in the presence of aluminum chloride gave 3,6-di-*tert*-butyl-9-(4-nitrophenyl)carbazole (**2**), which was subsequently reduced by Pd/C and hydrazine to 3,6-di-*tert*-butyl-9-(4-aminophenyl)carbazole (**3**). The synthesis procedure of Compound **3** is similar to that used by Zhu and Moore[22] and Chen et al.,[23] but with a different reducing condition. The synthesis of **3** also can be carried out by a different reaction sequence as reported by Koyuncu et al.[8(l)] The target dicarboxylic acid monomer **5** was successfully synthesized by alkaline hydrolysis of the dinitrile compound **4** resulting from the CsF-assisted *N*,*N*-diarylation of compound **3** with two equivalent amount of *p*-fluorobenzonitrile. The structures of all the synthesized compounds were confirmed by IR and NMR analyses. The FTIR spectra of intermediate compounds **1**–**4** and the target dicarboxylic acid monomer **5** can be seen in the Supporting Information (see Supporting Information Fig. S1). The nitro groups of Compounds **1** and **2** gave two characteristic bands at around 1594 and 1326 cm^{-1} (–NO_2 asymmetric and symmetric stretching). After Friedel–Crafts alkylation, the IR spectrum of Compound **2** gave aliphatic C–H stretching absorption around 2952 cm^{-1} (*t*-butyl C–H stretch). After reduction, the characteristic absorptions of the nitro group disappeared and the amino group showed the typical *N*–H stretching absorption pair in the region of 3300–3500 cm^{-1} as shown in the IR spectrum of Compound **3**. The IR spectrum of Compound **4** shows characteristic cyano peak at 2225 cm^{-1}. After hydrolysis, the characteristic absorption of the cyano group disappeared and the carboxylic acid group showed a typical carbonyl absorption band at 1687 cm^{-1} (C=O stretching) together with the appearance of broad band around 2400–3400 cm^{-1} (O–H stretching). The ^{1}H NMR and ^{13}C NMR spectra included in the Supporting Information (Supporting Information Figs. S2–S5) confirm the structures of precursor compounds **1**–**4**. Figure 1 illustrates the ^{1}H NMR and ^{13}C NMR spectra of dicarboxylic acid monomer **5**.

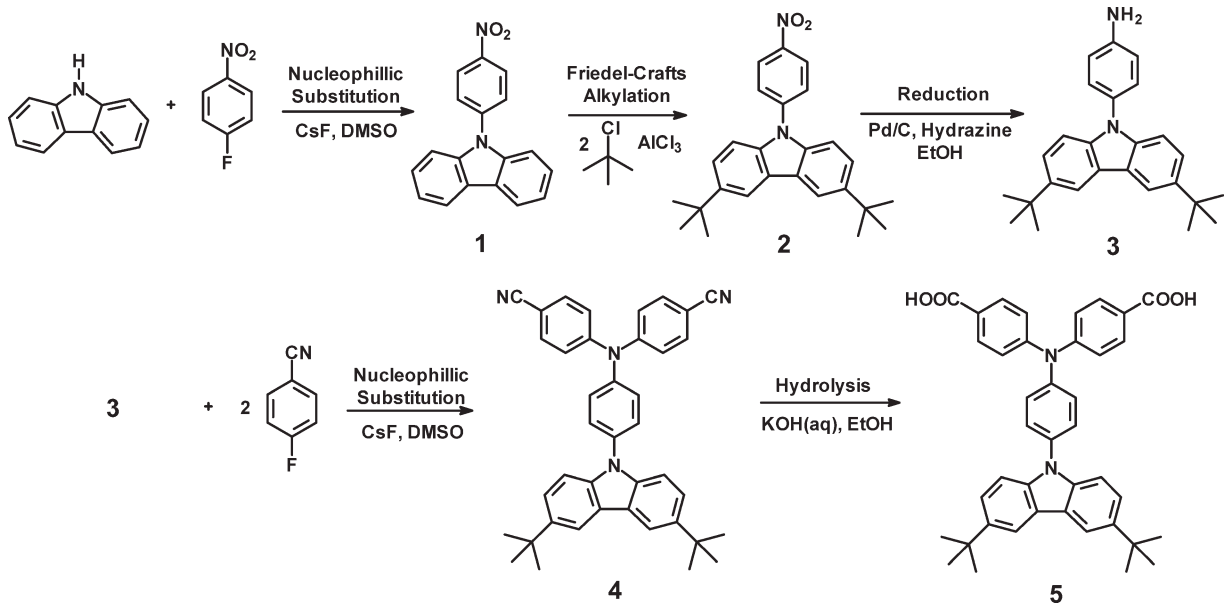

SCHEME 1 Synthesis route to target dicarboxylic acid monomer **5**.

Assignments of each carbon and proton are assisted by the 2D NMR spectra shown in the Supporting Information (Supporting Information Figs. S6 and S7), and the spectra agree well with the proposed molecular structures of **4** and **5**. The ^{13}C NMR spectra confirm that the cyano groups were completely converted into the carboxyl groups by the disappearance of the resonance peak for the cyano carbon at 118.7 ppm and by the appearance of the carbonyl peak at 166.7 ppm. Other important evidence of this change is the shifting of the carbon resonance signals of C-1 adjacent to the cyano or carboxyl group. The C-1 carbons of dinitrile compound **4** resonated at a higher field (106.3 ppm) than the other aromatic carbons because of the anisotropic shielding by the π electrons of C≡N. After hydrolysis, the resonance peak of C-1 shifted to a lower field (125.0 ppm) because of lacking of the anisotropic shielding field. In the H–H COSY spectrum for the aromatic region of dicarboxylic acid monomer **5**, the correlated pairs of AB doublets at 7.93/7.19 ppm and 7.62/7.36 ppm can be easily assigned to the protons a–d on the TPA core. The aromatic protons at the four positions (proton g) of the carbazole unit appear at the most downfield (8.29 ppm) as a singlet. Accordingly, other doublet signals at 7.19 and 7.38 ppm are assigned to the interconnected protons e and f, respectively. The signals appeared at 1.42 ppm in the ^{1}H NMR spectrum and at 34.4 ppm (a quaternary carbon) and 31.7 ppm (a methyl carbon) in the ^{13}C NMR spectrum are peculiar to the *tert*-butyl groups. These results suggest the successful preparation of the dicarboxylic acid monomer **5**.

Polymer Synthesis

According to the phosphorylation technique developed by Yamazaki et al.,[24] a series of novel aromatic polyamides (**7a**–**7f**) with (3,6-di-*tert*-butylcarbazol-9-yl)TPA units were synthesized from the dicarboxylic acid monomer **5** and aromatic diamines **6a**–**6f**[25] using TPP and pyridine as condensing agents (Scheme 2). All the polymerizations proceeded homogeneously throughout the reaction and afforded clear and highly viscous polymer solutions, which precipitated in a tough, fiberlike form when the resulting polymer solutions were slowly poured into methanol (see Supporting Information Fig. S8). As shown in Supporting Information Table S1, the obtained polyamides had inherent viscosities in the range of 0.40–0.63 dL/g and could be solution-cast into flexible and strong films, indicating the formation of high molecular weight polymers. This mechanical property is important for the further development of flexible optoelectronic devices. The weight-average molecular weights (M_w) of the THF-soluble polyamides **7c** and **7f** were 36,000 and 39,000 with polydispersity index (M_w/M_n) of 2.06 and 1.86, respectively. The formation of polyamides was also confirmed by IR and NMR spectroscopy. The representative IR spectrum for polyamide **7a** is included in the Supporting Information (Supporting Information Fig. S9), which shows the characteristic absorption bands of the amide group at around 1650 cm^{-1} (amide carbonyl) and 3300 cm^{-1} (*N*–H stretching). Figure 2 shows the ^{1}H NMR and COSY spectra of polyamide **7a** in DMSO-d_6. All the peaks could be readily assigned to the hydrogen atoms in the repeating unit. The resonance peak appearing at 10.35 ppm in the ^{1}H NMR spectrum also supports the formation of amide linkages.

Polymer Properties

Basic Characterization

The WAXD patterns of the polyamide films are shown in the Supporting Information (Supporting Information Fig. S10). These polymers exhibited an amorphous nature because of the bulky, packing-disruptive 3,6-di-*tert*-butyl-carbazolyl-substituted triphenylamino unit along the polymer backbone, which does not favor their close chain packing. The solubility behavior of polyamides **7a**–**7f** was tested qualitatively, and the results are summarized in the Supporting Information Table

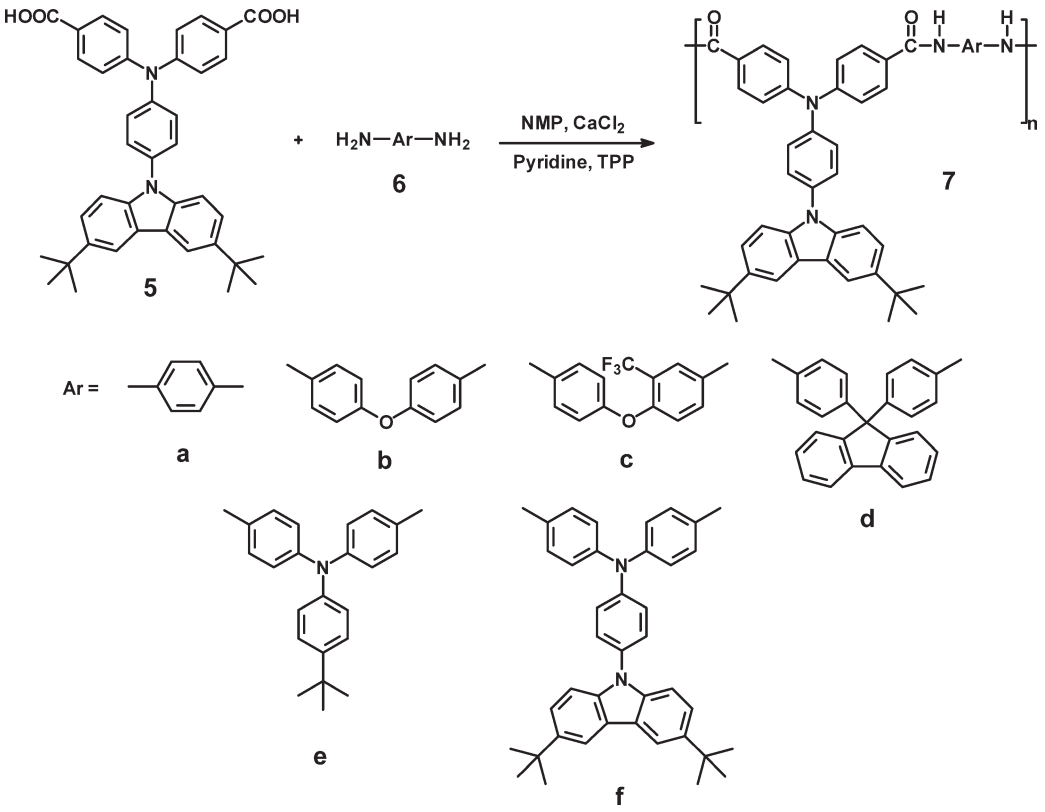

SCHEME 2 Synthesis of polyamides **7a**–**7f**.

S1. All the polyamides were highly soluble in polar solvents such as NMP, DMAc, and DMF, and the good solubility could be attributed in part to the introduction of propeller-shaped TPA moiety and bulky pendent 3,6-di-*tert*-butyl-carbazole substituents in the repeat unit, which decreases interchain interactions and increases the free volume. The polyamide **7c** showed a better solubility as compared with the CF_3-free **7b** analog. The solubility difference between **7c** and **7b** can be attributed to the effect of the large volume of CF_3 groups, which disrupted the regularity and dense chain packing leading to decreased interchain interactions. Thus, the excellent solubility makes these polymers potential candidates for practical applications by spin-coating or inkjet-printing processes to afford high-performance thin films for optoelectronic devices.

Thermal Properties

The thermal properties of all the polyamides were investigated by TGA, DSC, and TMA techniques, and the thermal behavior data are summarized in Table 1. Typical TGA curves of representative polyamide **7e** in both air and nitrogen atmospheres are illustrated in inset of Figure 3. All the polymers exhibited good thermal stability with insignificant weight loss up to 450 °C in both air and nitrogen atmospheres. The decomposition temperatures (T_d) at a 10% weight loss of the polyamides in nitrogen and air were recorded in the range of 486–546 and 482–541 °C, respectively. The mount of carbonized residue (char yield) of these polymers in nitrogen atmosphere was more than 66% at 800 °C. The high char yields of these polymers can be ascribed to their high aromatic content. The T_gs of all the polymers were measured to be in the range of 282–352 °C by DSC. All the polymers indicated no clear melting endotherms up to the decomposition temperatures on the DSC thermograms. This result also supports the amorphous nature of these polyamides. The softening temperatures (T_s; may be referred as apparent T_g) of the polymer film samples determined by the TMA method with a loaded penetration

TABLE 1 Thermal Properties of Polyamides

Polymer[a]	T_g (°C)[b]	T_s (°C)[c]	T_d at 10% Weight Loss (°C)[d]		Char Yield (wt %)[e]
			N_2	Air	
7a	335	303	518	503	71
7b	282	265	486	507	66
7c	293	282	492	482	66
7d	352	308	534	541	69
7e	323	295	505	518	68
7f	329	295	546	537	69

[a] The polymer film samples were heated at 300 °C for 30 min before all the thermal analyses.
[b] Midpoint temperature of the baseline shift on the second DSC heating trace (rate = 20 °C/min) of the sample after quenching from 400 to 50 °C (cooling rate = −200 °C/min) in nitrogen.
[c] Softening temperature measured by TMA with a constant applied load of 10 mN at a heating rate of 10 °C/min.
[d] Decomposition temperature at which a 10% weight loss was recorded by TGA at a heating rate of 20 °C/min and a gas flow rate of 20 cm^3/min.
[e] Residual weight percentage at 800 °C in nitrogen.

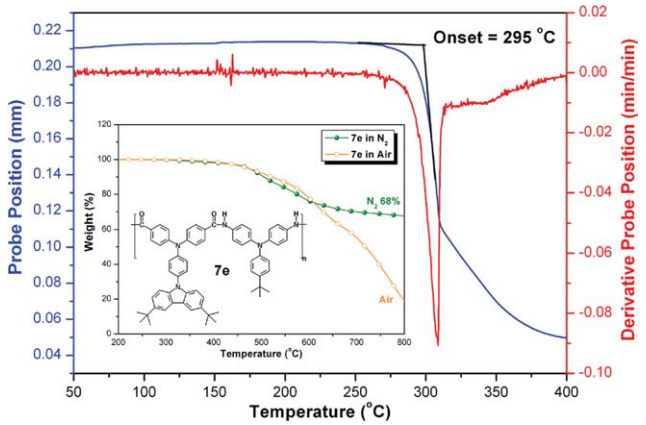

FIGURE 3 TMA and TGA curves of polyamide **7e** with a heating rate 10 and 20 °C/min, respectively.

probe are also listed in Table 1. They were obtained from the onset temperature of the probe displacement on the TMA trace. As a representative example, the TMA trace of polyamide **7e** is illustrated in Figure 3. In all cases, the T_s values of the polyamides obtained by TMA are lower than the T_g values measured by the DSC experiments. This may indicate that these polyamides exhibited a higher degree of plasticity near T_g because of the increased free volume caused by the bulky pendent groups. The thermal analysis results revealed that these polyamides exhibited excellent thermal stability, which in turn is beneficial to increase the service time in device application and enhance the morphological stability to the spin-coated film.

Optical Properties

The optical properties of the polyamides were investigated by UV–vis and PL spectroscopy. The results are summarized in Table 2. Figure 4 shows the UV–vis absorption and PL spectra of polyamides **7a–7d** in NMP. These polymers exhibited strong UV–vis absorption bands at 298 and 348–352 nm in NMP solutions, assignable to the π–π^* transitions of the carbazole and other π-conjugated moieties in the polymer backbone. In the solid state, the polyamides showed absorption characteristics similar to those observed in solutions, with low-energy absorption λ_{max} centered at 346–350 nm with absorption onsets at 406–421 nm corresponding to optical band gaps of 2.91–3.15 eV. Their PL spectra in dilute NMP solution showed maximum bands around 457–505 nm in the blue region with fluorescence quantum yields (Φ_F) ranging from 0.4% for **7e** to 32.8% for **7d**. The polyamide **7c** with the CF_3 substituents exhibited higher fluorescence quantum yields in comparison to the corresponding **7b** without the CF_3 substituents. This can be attributed to the presence of bulky, electron-withdrawing trifluoromethyl ($-CF_3$) substituents in polymer, which effectively restrict intra- and intermolecular charge transfer interactions. The highest Φ_F (32.8%) of **7d** can be attributed to the presence of bulky, rigid fluorene segments in polymer backbone. Although polymer **7a** exhibited a relatively lower Φ_F as compared to polymers **7b** to **7d**, its solution and solid film showed an obvious blue PL when irradiated by a standard laboratory UV lamp (see the photos shown on the top of Fig. 4). Polyamides **7e** and **7f** exhibited significantly less detectable fluorescence (Φ_F = 0.4-0.5%) when compared to the other polyamides. The low fluorescence can be attributed to the introduction of a TPA-containing structure in the diamine component, which may result in an increased nonradiative decay because of the greater conformational mobility.

TABLE 2 Optical Properties of Polyamides

	In Solution[a]			As Film		
Polymer	λ^{abs}_{max} (nm)	λ^{PL}_{max} (nm)	Φ_F (%)[b]	λ^{abs}_{max} (nm)	λ^{abs}_{onset} (nm)	λ^{PL}_{max} (nm)
7a	298, 352	457	2.9	298, 350	406	466
7b	298, 351	462	17.0	299, 347	401	457
7c	298, 348	466	21.3	298, 346	400	459
7d	298, 348	465	32.8	300, 347	394	461
7e	298, 351	505	0.4	298, 350	426	–
7f	298, 351	493	0.5	299, 349	421	–

[a] Measured in dilute solutions in NMP at a concentration of about 1×10^{-5} mol/L.
[b] Fluorescence quantum yield calculated in an integrating sphere with quinine sulfate as the standard (Φ_F = 54.6%).

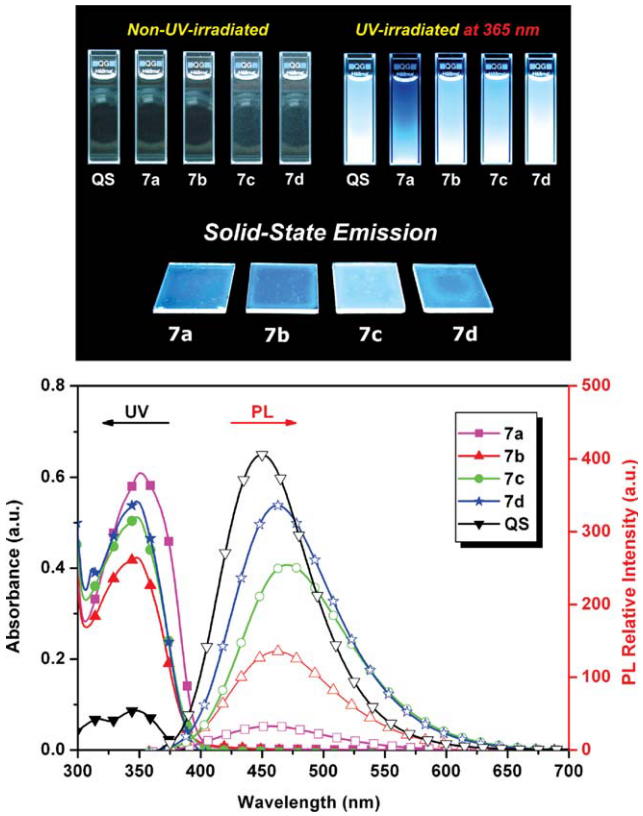

FIGURE 4 UV–vis absorption and PL spectra of the dilute solutions of polyamides **7a–7d** in NMP (1×10^{-5} M). Quinine sulfate dissolved in 1 M H_2SO_4 (aq.) with a concentration of 1×10^{-5} M as the standard (Φ_F = 54.6%). Photos show PL images of the solutions and thin films upon UV exposure (excited at 365 nm).

TABLE 3 Electrochemical Properties of Polyamides

	Oxidation Potential[a] (V)						HOMO[c] (eV)		LUMO[d] (eV)	
Polymer	E_{onset}	$E^{ox1}_{1/2}$	$E^{ox2}_{1/2}$	$E^{ox3}_{1/2}$	$E^{ox4}_{1/2}$	E_g[b] (eV)	E_{onset}	$E^{ox1}_{1/2}$	E_{onset}	$E^{ox1}_{1/2}$
7a	0.91	1.10	1.41	–	–	3.05	5.27	5.47	2.22	2.42
7′a	0.97	1.06	1.52[e]	–	–	3.07	5.33	5.42	2.26	2.35
7b	0.97	1.09	1.34	–	–	3.09	5.33	5.45	2.24	2.36
7c	0.92	1.04	1.32	–	–	3.10	5.28	5.40	2.18	2.30
7d	0.91	1.03	1.30	–	–	3.15	5.27	5.39	2.12	2.24
7′d	0.97	1.09	1.40[e]	–	–	3.12	5.33	5.44	2.21	2.32
7e	0.66	0.79	1.10	1.34	–	2.91	5.06	5.17	2.15	2.26
7f	0.65	0.71	1.14	1.25	1.38	2.95	5.07	5.20	2.12	2.25
7″a	0.68	0.83	1.18	–	–	3.07	5.04	5.19	1.97	2.12

[a] Oxidation potentials from cyclic votammograms (vs. Ag/AgCl in CH_3CN).
[b] Energy gap = 1240/Abs λ_{onset} of the polymer film.
[c] The HOMO energy levels were calculated from $E^{ox1}_{1/2}$ or E_{onset}, referenced to ferrocene (4.8 eV).
[d] LUMO = HOMO − E_g.
[e] Irreversible peak potential ($E_{p,a}$).

Structures of the referenced polyamides **7′a**, **7′d**, **7″a**:

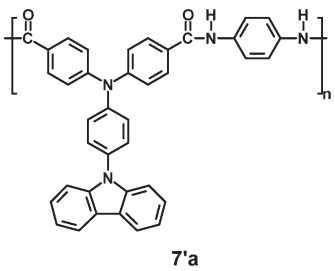

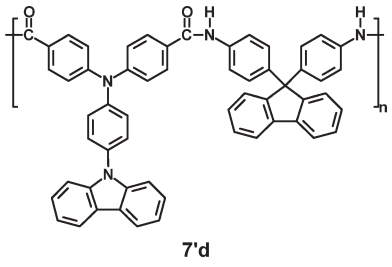

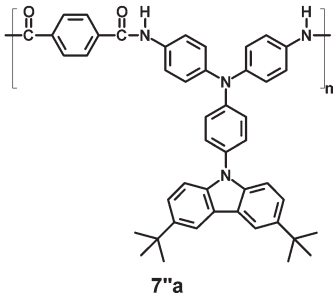

Electrochemical Properties

The electrochemical behavior of the polyamides was investigated by CV conducted for the cast film on an ITO-coated glass substrate as working electrode in dry acetonitrile (CH_3CN) containing 0.1 M of Bu_4NClO_4 as an electrolyte under nitrogen atmosphere. The derived oxidation potentials are summarized in Table 3. Figure 5(a) depicts the CV curves at different scan rates for polyamide **7d**, which was representative for the other **7a–7c** analogs. There are two reversible oxidation redox couples with half-wave potentials ($E_{1/2}$) of 1.03 and 1.30 V (at scan rate of 50 mV/s) for polyamide **7d**. The first oxidation wave can be due to the formation of triphenylamino radical cation, and the second one is attributable to the oxidation of the carbazole moiety. The two oxidation waves of **7d** are separated by about 270 mV, emphasizing the strong electronic coupling between the two redox amino centers of the TPA and carbazole units through the *p*-phenylene linker. A linear dependence of the peak currents as a function of scan rates confirmed both a nondiffusional redox process and a well-adhered electroactive polymer film [Fig. 5(b)]. Because of the stability of the films and good adhesion between the polymer and ITO substrate, **7d** exhibited excellent redox stability. Polyamide **7d** preserved good electroactivity after 10 repetitive scans between 0.0 and 1.5 V at a scan rate of 50 mV/s [Fig. 6(a)]. In contrast, the corresponding polyamide **7′d** without the *tert*-butyl groups on its carbazole unit rapidly lost redox reversibility in five cycles [Fig. 6(b)]. Thus, the incorporation of bulky *tert*-butyl groups on the active sites of the carbazole unit lends considerable stability of the present polyamides upon oxidation. According to these results, mechanisms of oxidation reactions for polyamides **7d** and **7′d** are proposed in Scheme 3. For polyamide **7d**, the two oxidation processes observed correspond to successive one electron removal from the TPA and carbazole moieties. These processes are highly reversible because of blockage of electrochemically active sites of the carbazole moiety with bulky *tert*-butyl group. As reported by Ambrose and coworkers in their pioneering work[26] devoted to anodic oxidation of carbazole and various *N*-substituted derivatives, ring–ring coupling is the predominant decay pathway. One possible coupling reaction of carbazylium radical cations to biscarbazylium dications shown in Scheme 3 can be used to explain the irreversible oxidation process occurring in polyamide **7′d**.

The redox stability enhancement effect due to *tert*-butyl substitution can be further confirmed by the CV curves of polyamide **7e** as illustrated in Figure 6(c). Polyamide **7e** exhibits three redox-active amino centers in each repeat unit and shows three corresponding quasireversible anodic redox couples. When comparing the differential pulse voltammogram (DPV) of **7e** with that of **7a** (see Fig. 7), we believe that the first oxidation peak at E_{pa} = 0.83 V appears to involve one electron loss from the TPA unit in the diamine component. This can be

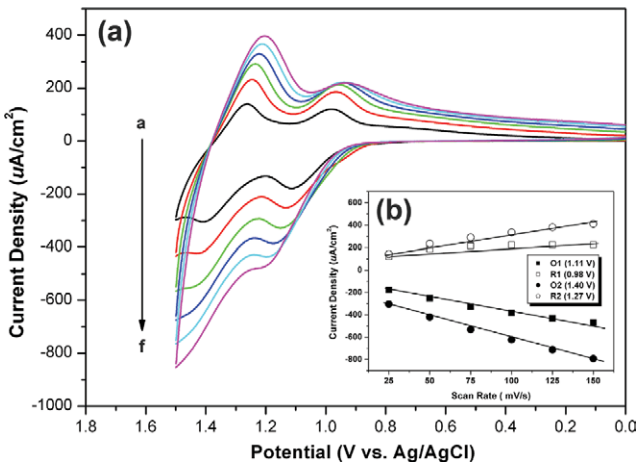

FIGURE 5 (a) Cyclic voltammograms of polyamide **7d** film on the ITO-coated glass substrate in 0.1 M Bu_4NClO_4/CH_3CN at different scan rates: (a) 25, (b) 50, (c) 75, (d) 100, (e) 125, and (f) 150 mV/s. (b) Relationship of anodic and cathodic current peaks as a function of scan rate. [Color figure can be viewed in the online issue, which is available at wileyonlinelibrary.com.]

rationalized because this TPA segment is more electron-rich and the amino unit becomes more easily oxidized. The second (E_{pa} = 1.11 V) and third (E_{pa} = 1.37 V) oxidation peaks are related to the electron losses from the TPA unit in the diacid component and the pendent carbazole moiety of polyamide **7e**. These potentials are similar to those associated with monocation and dication formations from the amino units in polyamide **7a**. The DPV diagrams of polyamides **7″a** (with isomeric repeat unit as that of **7a**) and **7f** are also shown in Figure 7. Apparently, the two oxidation processes observed for the referenced polyamide **7″a** at 0.84 V and 1.20 V attribute to successive one electron removal from the TPA and carbazole moieties in the diamine residue. Although polymer **7f** has four amino centers in its repeat unit, the second and third oxidations occurred almost simultaneously by a two-electron loss event. Therefore, these two oxidation waves merged (around 1.1–1.2 V) and became indistinguishable in the DPV diagram. Therefore, on the basis of the results from CV and DPV experiments, we propose the possible oxidation order for the amino centers of polyamides **7e** and **7f** as shown in Supporting Information Scheme S1. The simplified anodic oxidation pathways are depicted in Supporting Information Schemes S2 and S3. The other resonance forms for the TPA and carbazole radical cations are not shown, and a dication quinonediimine structure may form due to radical recombination.

The HOMO energy levels of the investigated polyamides were calculated from the oxidation onset potentials (E_{onset}) or half-wave potentials of the first oxidation wave ($E_{1/2}^{ox1}$) and by

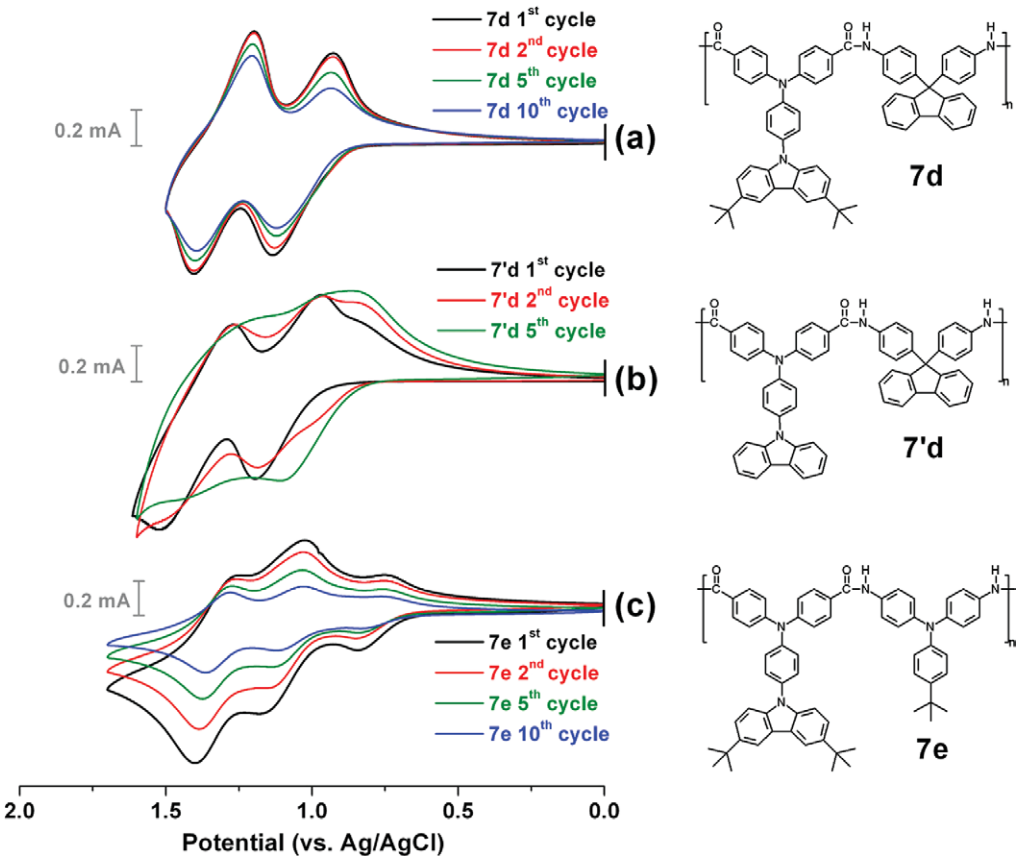

FIGURE 6 Repeated CV diagrams of (a) polyamide **7d**, (b) polyamide **7′d**, and (c) polyamide **7e** films on the ITO-coated glass substrate in 0.1 M Bu_4NClO_4/CH_3CN at a scan rate of 50 mV/s. [Color figure can be viewed in the online issue, which is available at wileyonlinelibrary.com.]

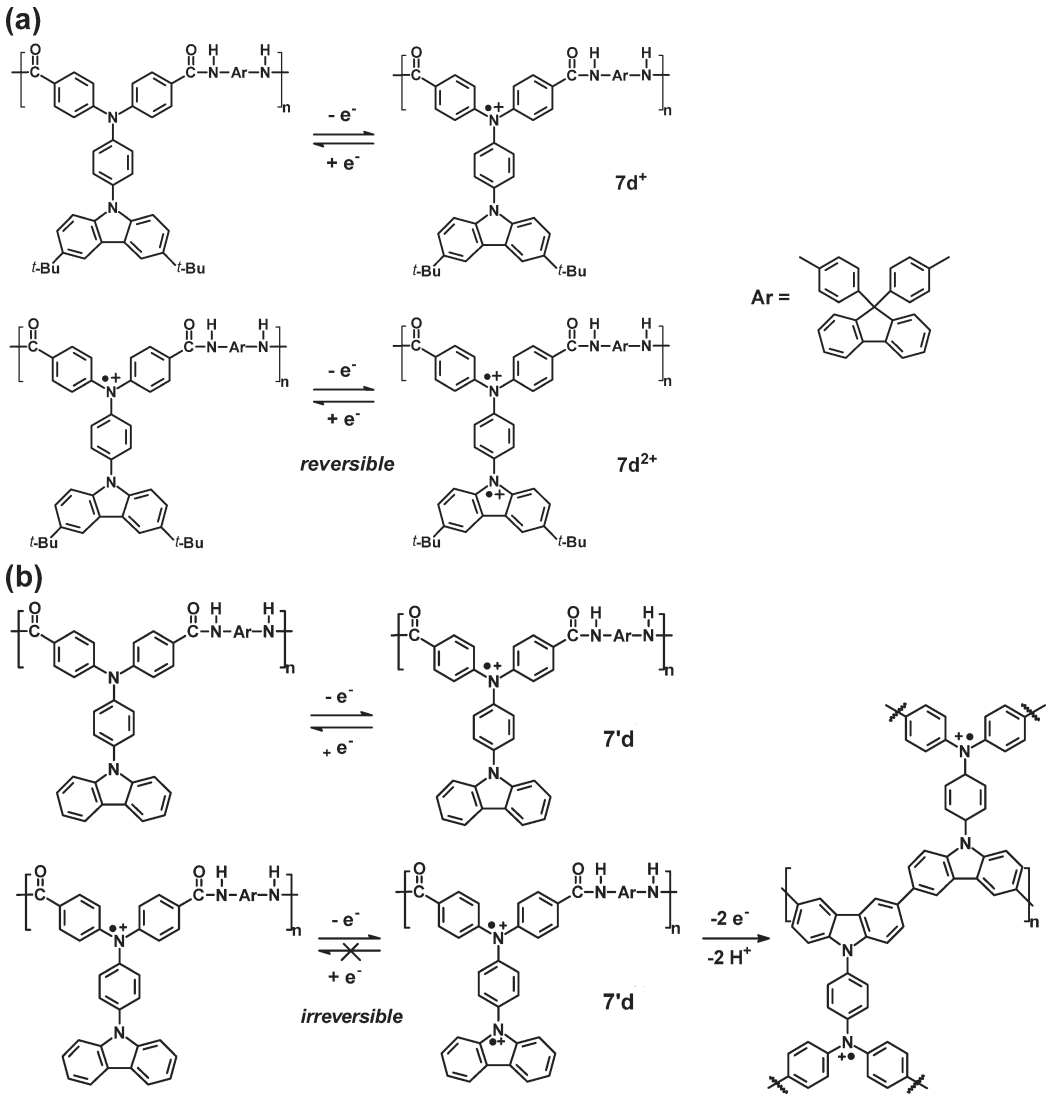

SCHEME 3 The anodic oxidation pathways of polyamides **7d** and **7′d**.

comparison with ferrocene (4.8 eV).[27] These data together with absorption spectra were then used to obtain the LUMO energy levels (Table 3). According to the HOMO and LUMO energy levels obtained, the polyamides in this study appear to be promising as hole injection and transport materials.

Spectroelectrochemistry

Spectroelectrochemical measurements were performed on films of polymers drop-coated onto ITO-coated glass slides immersed in electrolyte solution. The electrode preparations and solution conditions were identical to those used in the CV experiments. The change in absorption of polyamide **7a** film at various applied potentials is shown in Figure 8(a), which was representative for the other **7b–7d** counterparts. In the neutral form, at 0 V, polyamide **7a** exhibited strong absorption at wavelength around 350 nm, characteristic for π–π^* transitions, but it was almost transparent in the visible and near IR (NIR) regions. The band gap of polymer **7a** was calculated as 3.15 eV from the onset of the π–π^* transition. Upon applying potentials near the E^1_{pa} of **7a**, the absorption of π–π^* transition decreased while a new absorption peak at 414 nm and a broadband from 800 nm extended to 1100 nm in the NIR region grew up. Since the potentials examined are similar to the first anodic process, the spectral changes are assigned to the radical cation (polaron) formation arising from the oxidation of TPA unit. The absorption band in the NIR region may be attributed to an intervalence charge transfer (IVCT) between states in which the positive charge is centered at different amino centers (TPA and carbazole). The IVCT phenomenon of the family of triarylamines has been reported in literature.[28] Upon further oxidation at applied voltages to 1.4 V or above, the dication (bipolaron) band at 727 nm formed, which was also monitored synchronously with CV [Fig. 8(a), inset]. Concurrently, the IVCT band and the absorption peak at 414 nm decreased in intensity during this process. The observed electronic absorption changes in the film of **7a** at various potentials are fully reversible and are associated with strong color changes; indeed, they even can be seen readily by the naked eye. As shown in Figure 8(a), it can be seen that the film of polyamide **7a** switches from a transmissive neutral state

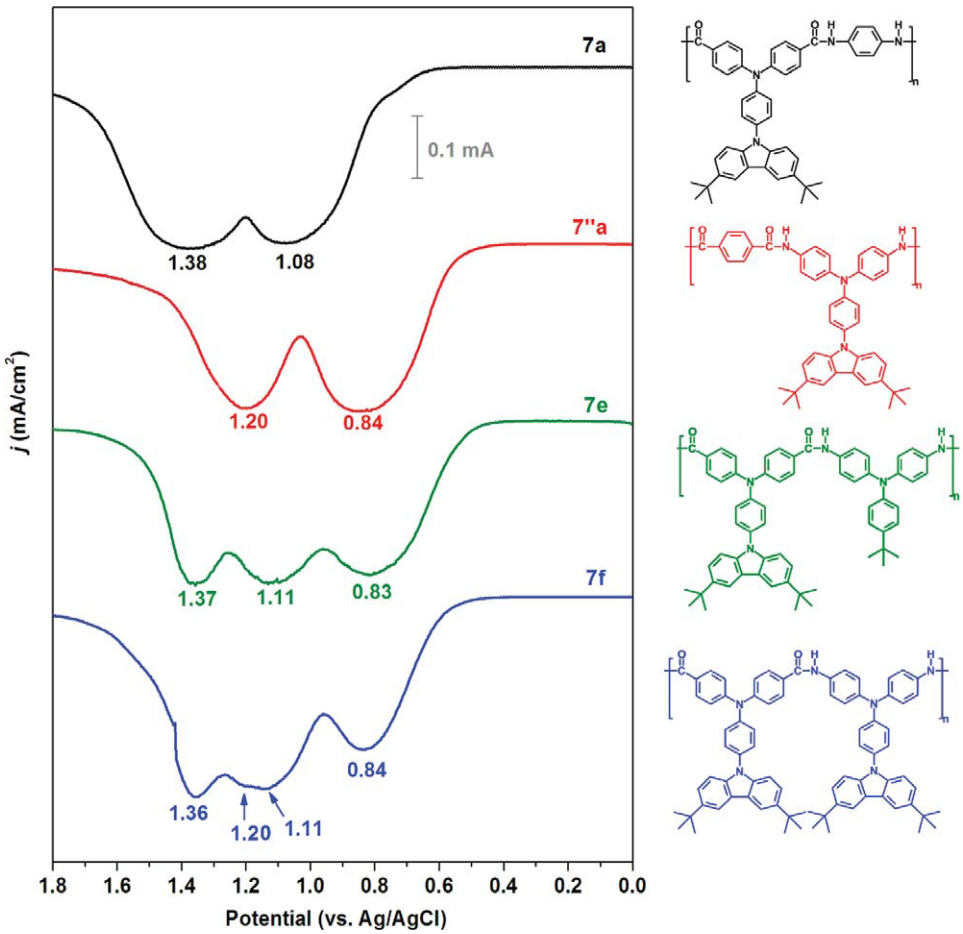

FIGURE 7 DPVs of the cast films of polyamides **7a**, **7″a**, **7e**, and **7f** on the ITO-coated glass substrate in 0.1 M Bu_4NClO_4/CH_3CN solution. Scan rate, 50 mV/s; pulse amplitude, 50 mV; pulse width, 50 ms; pulse period, 0.2 s. [Color figure can be viewed in the online issue, which is available at wileyonlinelibrary.com.]

(nearly colorless) to a highly absorbing semioxidized state (green) and a fully oxidized state (blue). Polyamide **7a** exhibited a very high optical contrast of transmittance change up to 85% at 727 nm for blue coloring. For a comparative study, the spectral changes of the referenced polyamide **7′a** without the *tert*-butyl substituents on the carbazole unit are presented in Figure 8(b). A similar spectral change was observed for polyamide **7′a** at early stage of oxidation (when the applied potential was below 1.3 V). The absorption around 714 nm started to appear when the applied potential was set at 1.7 V; however, the intensity is much lower than that observed for polyamide **7a** at the fully oxidized state. This result may be

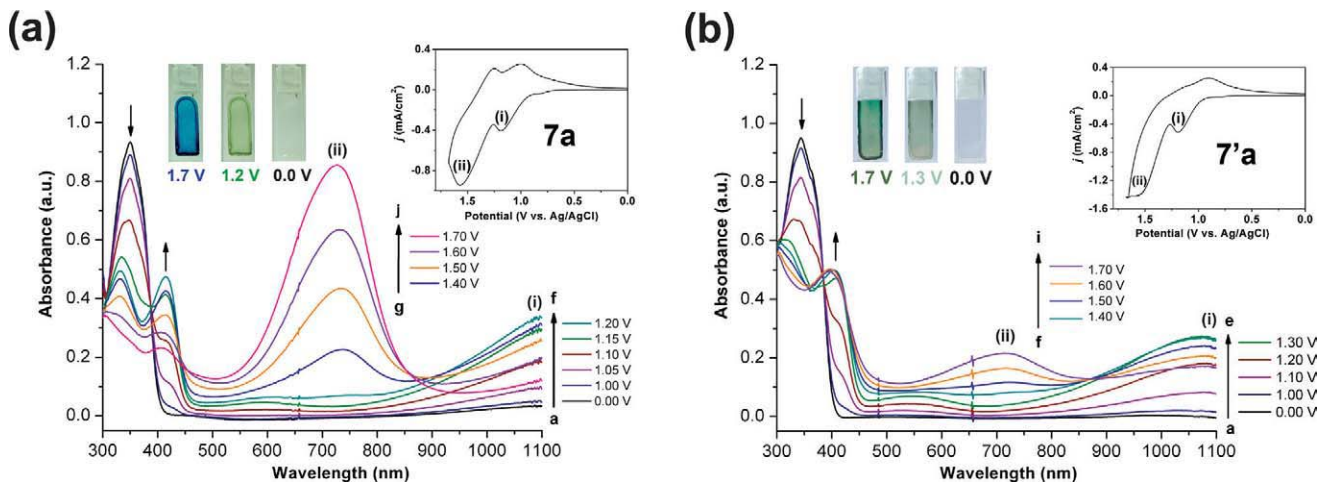

FIGURE 8 Spectral changes of the cast films of (a) polyamide **7a** and (b) polyamide **7′a** on an ITO-coated glass in 0.1 M Bu_4NClO_4/CH_3CN at various applied potentials (vs. Ag/AgCl). The insets show the color changes of the polymer films at indicated electrode potentials, together with their CV curves. [Color figure can be viewed in the online issue, which is available at wileyonlinelibrary.com.]

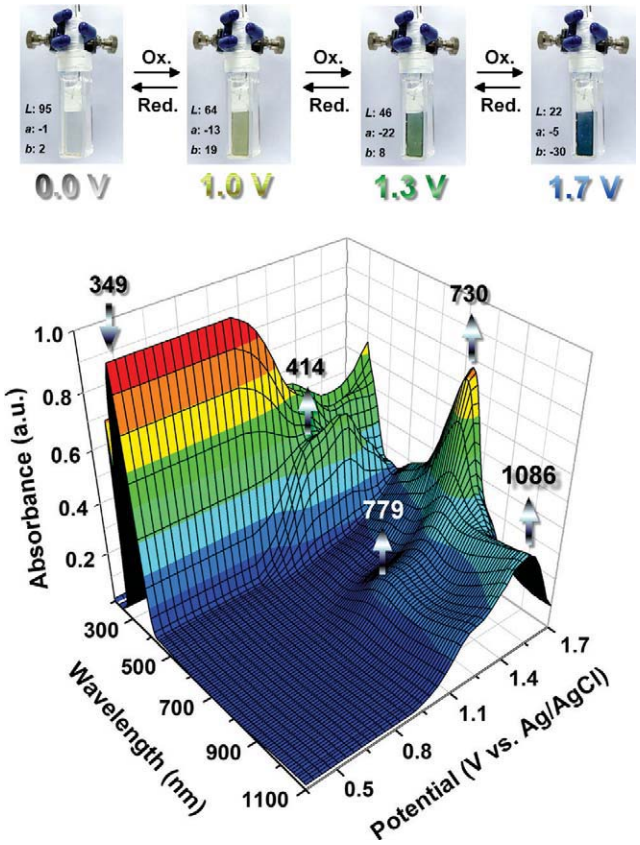

FIGURE 9 3D spectroelectrochemical behavior of polyamide **7f** thin film on the ITO-coated glass substrate (in CH_3CN containing 0.1 M Bu_4NClO_4 as the supporting electrolyte) from 0 to 1.7 V. The photo shows the color change of the film on an ITO electrode at indicated potentials. [Color figure can be viewed in the online issue, which is available at wileyonlinelibrary.com.]

explained by the irreversible second oxidation process associated with polyamide **7′a**. Thus, the effect of *tert*-butyl substitution on the enhancement of electrochemical and electrochromic reversibility and optical contrast ratio is very clear.

The spectral and color changes of the film of polyamide **7e** upon oxidation are illustrated in Figure S12(a), and the surface plot diagram for the absorbance–wavelength–applied potential correlations of this sample is depicted in Supporting Information Figure S12(b). Before electrical potential was applied, the colorless film of **7e** showed an intense absorption at 350 nm. By setting the potential to 1.0 V, the film showed a decrease in absorption at 350 nm with a concomitant appearance of a broad band having its maximum absorption wavelength at 813 nm. This spectral change corresponds to the first oxidation process of polyamide **7e** as shown in Supporting Information Scheme S2. This clearly evidences that the first oxidation originated from the TPA unit of the diamine residue in the **7e** main chain. When the electrode potential was adjusted to 1.3 V, the film gave new absorption bands at 419, 534, and 736 nm and NIR absorption from 850 to 1100 nm. We believe that the polymer has been oxidized to one having the bis(radical cation) repeating unit as the third structure shown in Supporting Information Scheme S2. When the applied potential was set at 1.7 V, a strong absorption band in the 600–850 nm region centering at around 728 nm was observed, whereas the intensity of the absorption peak at 419 nm and the NIR absorption gradually decreased. This result indicated the occurrence of the third oxidation. The film of polyamide **7e** displayed a multielectrochromic behavior with coloration change from colorless (L: 94; a: −2; b: 5) to green (L: 67; a: −30; b: 5), red–purple (L: 46; a: 9; b: 1), and dark blue (L: 17; a: −5; b: −11) along with increasing of the applied potential. Similar to that of polyamide **7e**, the neutral-form polyamide **7f** showed intense absorption in the UV region peaked at 349 nm (see Fig. 9). By setting the potential over 1.0 V, the film gave new absorption bands in the visible and NIR regions, with coloration changes from colorless (L: 95; a: −1; b: 2) to yellowish green (L: 64; a: −13; b: 19), green (L: 46; a: −22; b: 8), and blue (L: 22; a: −5; b: −30). As the polymer film of **7f** was oxidized at 1.0–1.3 V, the π–π^* transition band at 349 nm began to diminish concurrently with intensifying of new absorption bands at 414 and 779 nm, and the film turned to a yellowish green or green color at low doping levels. Upon further oxidation at 1.7 V, the absorption at 414 nm dropped, and a new strong absorption band peaked at 730 nm arose; the film turned to blue. The spectral changes had apparently arisen from the sequential oxidation processes of the amino centers in the two different carbazol-9-yl-substituted TPA segments in the main chain of this polyamide. The possible anodic pathways of polyamide **7f** are proposed in

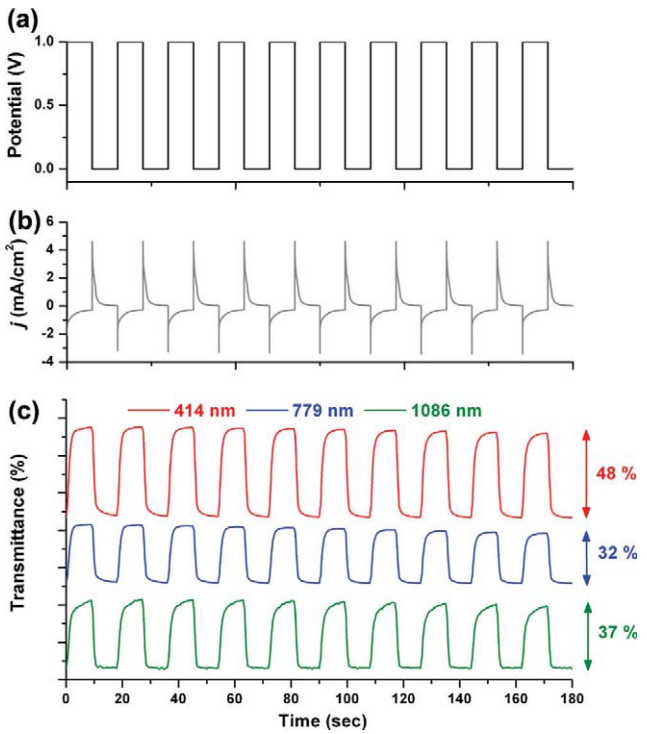

FIGURE 10 (a) Potentials and (b) current densities during switching studies. (c) Optical transmittance change monitored at 414, 779, and 1086 nm for polyamide **7f** thin film on ITO-glass slide in 0.1 M Bu_4NClO_4/CH_3CN. [Color figure can be viewed in the online issue, which is available at wileyonlinelibrary.com.]

Supporting Information Scheme S3, in which the second and third oxidation processes may take place simultaneously as shown by the DPV experiment.

Electrochromic Switching

Optical switching studies were examined for probing changes in transmittance with time while repeatedly stepping the potential between neutral and oxidized states. The polymer film was cast onto an ITO-coated glass slides in the same manner as described earlier. We extracted the electrochromic parameters of the polyamides **7e** and **7f** films by analysis of transmittance change decrement or increment of the absorption at 813 nm (for **7e**) and 414, 779, and 1086 nm (for **7f**) with respect to time while the potential was switched stepwise between the neutral (0 V) and the oxidized state at + 1.0 V with a residence time of 9 s. During this measurement, the percent transmittance (%T) value at the indicated wavelengths was measured using a UV–vis–NIR spectrophotometer. The results for the first 10 cycles are shown in Figure 10 and Supporting Information Figure S13. The optical contrast measured as the difference between %T of polyamide **7e** at 0 and 1.0 V was found to be 47% at 813 nm. The optical contrasts for polyamide **7f** were found to be 48, 32, and 37% for 414, 779, and 1086 nm, respectively. After over hundreds of cyclic scans between 0.0 and 1.0 V, the polymer films still exhibited good electrochemical and electrochromic reversibility. CE ($\eta = \Delta OD/Q$)[1] was measured by monitoring the amount of ejected charge (Q) as a function of the change in optical density (ΔOD) of the polymer film. The CE of **7e** (at 813 nm) and **7f** (at 414 nm) films was calculated to be 100 and 104 cm^2/C, respectively.

CONCLUSIONS

The new carbazole and TPA-containing aromatic dicarboxylic acid monomer, 4,4′-dicarboxy-4″-(3,6-di-*tert*-butylcarbazol-9-yl)TPA was successfully synthesized in high purity and good yield from readily available reagents. Aromatic polyamides bearing redox-active TPA and carbazole units were readily prepared from the newly synthesized dicarboxylic acid monomer and various aromatic diamines by the phosphorylation polyamidation technique. Because of the introduction of three-dimensional TPA units and bulky 3,6-di-*tert*-butylcarbazole pendent groups in polymer backbone, all the polymers were amorphous, had good solubility in many polar aprotic solvents, and exhibited excellent film-forming ability. Some of the polymers also exhibited strong fluorescence both in film and in solution with quantum yield up to 32%. In addition to high T_g values and good thermal stability, all the obtained polyamides also revealed good electrochemical and electrochromic stability along with multielectrochromic behavior. By substitution of the electrochemically active C3 and C6 sites of the carbazole unit with sterically bulky *tert*-butyl groups, the new polyamides exhibit greatly enhanced electrochemical stability and electrochromic performance in comparison with previously reported analogs without *tert*-butyl substituents on the carbazole moiety. Such prominent features make these processable polymers amenable for optoelectronic applications such as OLEDs and electrochromic devices.

The authors greatly appreciate the support of this research by the National Science Council of Taiwan (Republic of China).

REFERENCES AND NOTES

1 Monk, P. M. S.; Mortimer, R. J.; Rosseinsky, D. R. Electrochromism and Electrochromic Devices; Cambridge University Press: Cambridge, UK, 2007.

2 (a) Rosseinsky, D. R.; Montimer, R. J. Adv Mater 2001, 13, 783–793; (b) Michaelis, A.; Berneth, H.; Haarer, D.; Kostromine, S.; Neigl, R.; Schmidt, R. Adv Mater 2001, 13, 1825–1828; (c) Heuer, H. W.; Wehrmann, R.; Kirchmeyer, S. Adv Funct Mater 2002, 12, 89–94; (d) Sonmez, G.; Sonmez, H. B. J Mater Chem 2006, 16, 2473–2477; (e) Anderson, P.; Forchheimer, R.; Tehrani, P.; Berggren, M. Adv Funct Mater 2007, 17, 3074–3082; (f) Baetens, R.; Jelle, B. P.; Gustavsen, A. Sol Energy Mater Sol Cells 2010, 94, 87–105; (g) Beaupre, S.; Breton, A.-C.; Dumas, J.; Leclerc, M. Chem Mater 2009, 21, 1504–1513.

3 (a) Mortimer, R. J. Chem Soc Rev 1997, 26, 147–156; (b) Mortimer, R. J. Electrochim Acta 1999, 44, 2971–2981; (c) Rowley, N. M.; Mortimer, R. J. Sci Prog 2002, 85, 243–262; (d) Mortimer, R. J.; Dyer, A. L.; Reynolds, J. R. Displays 2006, 27, 2–18.

4 (a) Baeck, S.-H.; Choi, K.-S.; Jaramillo, T. F.; Stucky, G. D.; McFarland, E. W. Adv Mater 2003, 15, 1269–1273; (b) Lee, S.-H.; Deshpande, R.; Parilla, P. A.; Jones, K. M.; To, B.; Mahan, H.; Dillon, A. C. Adv Mater 2006, 18, 763–766; (c) Niklasson, G. A.; Granqvist, C. G. J Mater Chem 2007, 17, 127–156.

5 (a) Sonmez, G. Chem Commun 2005, 5251–5259; (b) Beaujuge, P. M.; Reynolds, J. R. Chem Rev 2010, 110, 268–320; (c) Patra, A.; Bendikov, M. J Mater Chem 2010, 20, 422–433.

6 (a) Welsh, D. M.; Kumar, A.; Morvant, M. C.; Reynolds, J. R. Synth Met 1999, 102, 967–968; (b) Groenendaal, L.; Jonas, F.; Freitag, D.; Pielartzik, H.; Reynolds, J. R. Adv Mater 2000, 12, 481–494; (c) Groenendaal, L.; Zotti, G.; Aubert, P.-H.; Waybright, S. M.; Reynolds, J. R. Adv Mater 2003, 15, 855–879; (d) Argun, A. A.; Aubert, P.-H.; Thompson, B. C.; Schwendeman, I.; Gaupp, C. L.; Hwang, J.; Pinto, N. J.; Tanner, D. B.; MacDiarmid, A. G.; Reynolds, J. R. Chem Mater 2004, 16, 4401–4412.

7 (a) Schottland, P.; Zong, K.; Gaupp, C. L.; Thompson, B. C.; Thomas, C. A.; Giurgiu, I.; Hickman, R.; Abboud, K. A.; Reynolds, J. R. Macromolecules 2000, 33, 7051–7061; (b) Zong, K.; Reynolds, J. R. J Org Chem 2001, 66, 6873–6882; (c) Sonmez, G.; Schwendeman, I.; Schottland, P.; Zong, K.; Reynolds, J. R. Macromolecules 2003, 36, 639–647; (d) Walczak, R. M.; Reynolds, J. R. Adv Mater 2006, 18, 1121–1131; (e) Walczak, R. M.; Jung, J.-H.; Cowart, J. S., Jr.; Reynolds, J. R. Macromolecules 2007, 40, 7777–7785.

8 (a) Sonmez, G.; Meng, H.; Wudl, F. Chem Mater 2004, 16, 574–580; (b) Sonmez, G.; Sonmez, H. B.; Shen, C. K. F.; Jost, B. W.; Rubin, Y.; Wudl, F. Macromolecules 2005, 38, 669–675; (c) Wu, C.-G.; Lu, M.-I.; Chang, S.-J.; Wei, C.-S. Adv Funct Mater 2007, 17, 1063–1070; (d) Durmus, A.; Gunbas, G. E.; Toppare, L. Chem Mater 2007, 19, 6247–6251; (e) Gunbas, G. E.; Durmas, A.; Toppare, L. Adv Mater 2008, 20, 691–695; (f) Gunbas, G. E.; Durmus, A.; Toppare, L. Adv Funct Mater 2008, 18, 2026–2030; (g) Balan, A.; Gunas, G.; Durmus, A.; Toppare, L. Chem Mater 2008, 20, 7510–7513; (h) Cihaner, A.; Algi, F. Adv Funct Mater 2008, 18, 3583–3589; (i) Pamuk, M.; Tirkes, S.; Cihaner, A.; Algi, F. Polymer 2010, 51, 62–68; (j) Icli, M.; Pamuk, M.; Algi, F.; Onal, A. M.; Cihaner, A. Chem Mater 2010, 22, 4034–4044; (k) Koyuncu, S.; Kus, M.; Demic, S.; Kaya, I.; Ozdemir, E.; Icli, S. J

Polym Sci Part A: Polym Chem 2008, 46, 1974–1989; (l) Koyuncu, S.; Zafer, C.; Sefer, E.; Koyuncu, F. B.; Demic, S.; Kaya, I.; Ozdemir, E.; Icli, S. Synth Met 2009, 159, 2013–2021; (m) Is, O. D.; Koyuncu, F. B.; Koyuncu, S.; Ozdemir, E. Polymer 2010, 51, 1663–1669.

9 Yang, H. H. Kevlar Aramid Fiber; Wiley: Chichester, UK, 1993.

10 (a) Hsiao, S.-H.; Huang, T.-L. J Polym Sci Part A: Polym Chem 2002, 40, 947–957; (b) Liou, G.-S.; Hsiao, S.-H. J Polym Sci Part A: Polym Chem 2002, 40, 1781–1789; (c) Hsiao, S.-H.; Chang, Y.-M. J Polym Sci Part A: Polym Chem 2004, 42, 4056–4062; (d) San-Jose, N.; Gomez-Valdemoro, A.; Estevez, P.; Garcia, F. C.; Serna, F.; Garcia, J. M. Eur Polym J 2008, 44, 3578–3587; (e) Ghaemy, M.; Amini Nasab, S. M. React Funct Polym 2010, 70, 306–313; (f) Espeso, J. F.; Lozano, A. E.; de la Campa, J. G.; Garcia-Yoldi, I.; de Abajo, J. J Polym Sci Part A: Polym Chem 2010, 48, 1743–1751.

11 Garcia, J. M.; Garcia, F. C.; Serna, F. S.; de la Pena, J. L. Prog Polym Sci 2010, 35, 623–686 and the references cited herein.

12 (a) Thelakkat, M. Macromol Mater Eng 2002, 287, 442–461; (b) Shirota, Y.; Kageyama, H. Chem Rev 2007, 107, 953–1010.

13 (a) Liang, F.; Kurata, T.; Nishide, H.; Kido, J. J Polym Sci Part A: Polym Chem 2005, 43, 5765–5773; (b) Kim, Y.-H.; Zhao, Q.; Kwon, S.-K. J Polym Sci Part A: Polym Chem 2006, 44, 172–182; (c) Zhao, Q.; Kim, Y.-H.; Mai Dang, T. T.; Shin, D.-C.; You, H.; Kwon, S.-K. J Polym Sci Part A: Polym Chem 2007, 45, 341–347; (d) Chuang, C.-Y.; Shih, P.-I; Chien, C.-H.; Wu, F.-I.; Shu, C.-F. Macromolecules 2007, 40, 247–252; (e) Mikroyannidis, J. A.; Gibbons, K. M.; Kulkarni, A. P.; Jenekhe, S. A. Macromolecules 2008, 41, 663–674; (f) Park, J. H.; Huh, J. O.; Do, Y.; Lee, M. H. J Polym Sci Part A: Polym Chem 2008, 46, 5816–5825; (g) Park, J. H.; Yun, C.; Park, M. H.; Do, Y.; Yoo, S.; Lee, M. H. Macromolecules 2009, 42, 6840–6843; (h) Hsieh, B.-Y.; Chen, Y. J Polym Sci Part A: Polym Chem 2009, 47, 1553–1566; (i) Nursalim, G.; Chen, Y. Polymer 2010, 51, 3187–3195.

14 (a) Leung, M.-k.; Chou, M.-Y.; Su, Y. O.; Chiang, C. L.; Chen, H.-L.; Yang, C. F.; Yang, C.-C.; Lin, C.-C.; Chen, H.-T. Org Lett 2003, 5, 839–842; (b) Beaupre, S.; Dumas, J.; Leclerc, M. Chem Mater 2006, 18, 4011–4018; (c) Otero, L.; Sereno, L.; Fungo, F.; Liao, Y.-L.; Lin, C.-Y.; Wong, K.-T. Chem Mater 2006, 18, 3495–3502; (d) Natera, J.; Otero, L.; Sereno, L.; Fungo, F.; Wang, N.-S.; Tsai, Y.-M.; Hwu, T.-Y.; Wong, K.-T. Macromolecules 2007, 40, 4456–4463.

15 (a) Cheng, S.-H.; Hsiao, S.-H.; Su, T.-H.; Liou, G.-S. Macromolecules 2005, 38, 307–316; (b) Hsiao, S.-H.; Chang, Y.-M.; Chen, H.-W.; Liou, G.-S. J Polym Sci Part A: Polym Chem 2006, 44, 4579–4592; (c) Liou, G.-S.; Hsiao, S.-H.; Huang, N.-K.; Yang, Y.-L. Macromolecules 2006, 39, 5337–5346; (d) Chang, C.-W.; Liou, G.-S.; Hsiao, S.-H. J Mater Chem 2007, 17, 1007–1015; (e) Hsiao, S.-H.; Liou, G.-S.; Kung, Y.-C.; Yen, H.-J. Macromolecules 2008, 41, 2800–2808; (f) Kung, Y.-C.; Liou, G.-S.; Hsiao, S.-H. J Polym Sci Part A: Polym Chem 2009, 47, 1740–1755; (g) Hsiao, S.-H.; Liou, G.-S.; Wang, H.-M. J Polym Sci Part A: Polym Chem 2009, 47, 2330–2343; (h) Hsiao, S.-H.; Liou, G.-S.; Kung, Y.-C.; Chang, Y.-M. J Polym Sci Part A: Polym Chem 2010, 48, 2798–2809.

16 (a) Chen, J. P.; Natansohn, A. Macromolecules 1999, 32, 3171–3177; (b) Morin, J.-F.; Leclerc, M.; Ades, D.; Siove, A. Macromol Rapid Commun 2005, 26, 761–778.

17 (a) Grazulevicius, J. V.; Strohriegl, P.; Pielichowski, J.; Pielichowski, K. Prog Polym Sci 2003, 28, 1297–1353; (b) Blouin, N.; Leclerc, M. Acc Chem Res 2008, 41, 1110–1119; (c) Boudreault, P.-L. T.; Beaupre, S.; Leclerc, M. Polym Chem 2010, 1, 127–136.

18 Tsai, M.-H.; Lin, H.-W.; Su, H.-C.; Ke, T.-H.; Wu, C.-c.; Fang, F.-C.; Liao, Y.-L.; Wong, K.-T.; Wu, C.-I. Adv Mater 2006, 18, 1216–1220.

19 Yang, C.-P.; Chen, R.-S.; Chen, K.-H. Colloid Polym Sci 2003, 281, 505–515.

20 Schaerlaekens, M.; Hendrickx, E.; Hameurlaine, A.; Dehaen, W.; Persoons, A. Chem Phys 2002, 277, 43–52.

21 Demas, J. N.; Crosby, G. A. J Phys Chem 1971, 75, 991–1024.

22 Zhu, Z.; Moore, J. S. J Org Chem 2000, 65, 116–123.

23 Chen, Y.-C.; Huang, G.-S.; Hsiao, C.-C.; Chen, S.-A. J Am Chem Soc 2006, 128, 8549–8558.

24 (a) Yamazaki, N.; Higashi, F.; Kawabata, J. J Polym Chem Polym Chem Ed 1974, 12, 2149–2155; (b) Yamazaki, N.; Matsumoto, M.; Higashi, F. J Polym Sci Polym Chem Ed 1975, 13, 1373–1380.

25 A detailed description of the synthesis of 4,4′-diamino-4″-(3,6-di-*tert*-butylcarbazol-9-yl)TPA (diamine **6f**) and its based polyamides and polyimides is at hand and will be published in the near future: Liao, S.-H., Dissertation, Tatung University, Taiwan, 2007.

26 (a) Ambrose, J. F.; Nelson, R. F. J Electrochem Soc 1968, 115, 1159–1164; (b) Ambrose, J. F.; Capenter, L. L.; Nelson, R. F. J Electrochem Soc 1975, 122, 876–894.

27 Shen, J.-Y.; Lee, C.-Y.; Huang, T.-H.; Lin, J.-T.; Tao, Y.-T.; Chien, C.-H.; Tsai, C. J Mater Chem 2005, 15, 2455–2463.

28 (a) Lambert, C.; Noll, G. J Am Chem Soc 1999, 121, 8434–8442; (b) Lambert, C.; Noll, G. Angew Chem Int Ed 1998, 37, 2107–2110; (c) Lambert, C.; Noll, G. Synth Met 2003, 139, 57–62; (d) Chou, M.-Y.; Leung, M.-k.; Su, Y. O.; Chiang, C. L.; Lin, C.-C.; Liu, J.-H.; Kuo, C.-K.; Mou, C.-Y. Chem Mater 2004, 16, 654–661; (e) Chiang, C. C.; Chen, H.-C.; Lee, C.-s.; Leung, M.-k.; Lin, K.-R.; Hsieh, K.-H. Chem Mater 2008, 20, 540–552.